RSC Advances

ROYAL SOCIETY OF CHEMISTRY

www.rsc.org/advances

The sulphidation temperature has a pronounced influence on both textural and structural properties of the NiO-MoO_3/γ-Al_2O_3 catalysts for sulphur-resistant methanation.

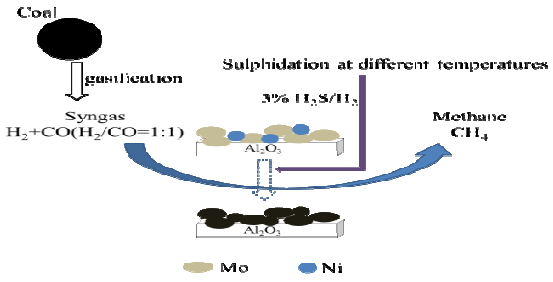

RSC Advances

RSCPublishing

ARTICLE

Effect of sulphidation temperature on the performance of NiO-MoO_3/γ-Al_2O_3 catalysts for sulphur-resistant methanation

Cite this: DOI: 10.1039/x0xx00000x

Received xxth Xxxx 20xx,
Accepted xxth Xxxx 20xx

DOI: 10.1039/x0xx00000x

www.rsc.org/

Baowei Wang*, Zongyuan Hu, Sihan Liu, Minhong Jiang, Yuqin Yao, Zhenhua Li, Xinbin Ma*

The effect of the sulphidation temperature on the activity and selectivity of a NiO-MoO_3/γ-Al_2O_3 catalyst for sulphur-resistant methanation was systematically investigated. The prepared catalysts were subsequently characterised by N_2-physisorption, temperature-programmed sulphidation, X-ray diffraction, Raman spectroscopy, X-ray photoelectron spectroscopy and transmission electron microscopy. The results obtained from characterisation demonstrated that the $NiMoO_4$ species in the NiO-MoO_3/γ-Al_2O_3 catalyst would be sulphided when the sulphidation temperature was at or above 300 °C. Evaluation of the catalysts in sulphur-resistant methanation from syngas indicated that the sample sulphided at 400 °C has the highest catalytic activities likelihood of possessing greater NiMoS type I structure. The catalytic activity decreased when the sulphidation temperature was above 400 °C. This decrease was primarily caused by the formation of MoS_2 crystals and the progressive transformation of the NiMoS phase with increasing the sulphidation temperature. The NiMoS type II structure did not display good performance for sulphur-resistant methanation because it resulted in the over-sulphidation of the NiMoS structure to form crystalline MoS_2, which exhibited lower methanation activity.

Introduction

Recently, the study and development of synthetic natural gas (SNG) production has attracted increasingly more attention and entered an era of rapid development since environmental contamination and energy shortage crises.[1] Notably, the production of SNG is a relatively reasonable and clean way to utilise coal adequately. Methanation is a key reaction for producing SNG from syngas. Transition metals, such as nickel, are commonly used as methanation catalysts because they possess high methanation activity. Not only does this type of catalysts show a high degree of CO conversion, but also contain good selectivity to CH_4.[2, 3] The methanation reaction over Ni-based catalysts occurs as follows:

$$CO + 3H_2 \rightarrow CH_4 + H_2O \quad (1)$$

As is evident in equation (1), methanation reactions over Ni-based catalysts require a H_2/CO molar ratio of no less than 3:1. However, for most coal gasification processes, it is almost impossible to generate syngas with such a high H_2/CO ratio. Thus, the adjustment of the H_2/CO ratio is inevitably performed via a water-gas shift (WGS) reaction in syngas:

$$CO + H_2O \rightarrow CO_2 + H_2 \quad (2)$$

which is an expensive process. By using the MoS_2-based catalysts, the following methanation reaction is proposed.

$$2CO + 2H_2 \rightarrow CH_4 + CO_2 \quad (3)$$

MoS_2-based catalyst can significantly reduce the cost of methanation reactions from syngas and react at low H_2/CO ratios (H_2/CO=1:1). Moreover, it is widely recognised that the MoS_2-based catalyst exhibits sulphur-tolerance ability during methanation, whereas Ni-based catalysts are very sensitive to sulphur poisoning.[4] Hence, this sensitivity leads to certain operating limitations of Ni-based catalyst, and also increases the attention for MoS_2-based catalysts in industry.

To date, due to the specific properties of MoS_2-based catalysts, such as high catalytic activity and sulphur-resistant ability, these catalysts have been broadly applied to various hydrotreating reactions, such as hydrodesulphurisation, the Fischer-Tropsch synthesis and alcohol synthesis.[5-8] The active phase of the MoS_2-based catalyst has been recognised extensively as MoS_2, which is formed by sulphiding oxidic precursor. Although the sulphidation of the oxidic precursor can occur under reaction conditions, its catalytic performance completely relies on the raw materials used and optimal operational conditions. For catalysts prepared from precursors containing oxygen, sulphidation plays a key role in determining the catalytic performances of such catalysts.[9-11] It is therefore essential to adjust well-controlled sulphided conditions for the MoS_2-based catalyst in order to obtain better catalytic performance.[12] Following sulphidation, whether molybdenum oxysulphide or MoS_2 exists on the catalyst must be determined, as the species present is correlated with the activity. Hence, it is believed that Mo-based sulphides might be promising catalysts for methanation.

Unlike monometallic MoS_2-based catalysts, bimetallic MoS_2-based catalysts, such as CoO-MoO_3/γ-Al_2O_3 and NiO-MoO_3/γ-Al_2O_3, show higher catalytic activity in hydrotreating reactions.[13-15] Sulphided Ni-Mo and Co-Mo catalysts supported on Al_2O_3 have been used extensively in several hydrotreating processes, such as hydrodesulphurisation (HDS), hydro-denitrogenation (HDN), hydrodeoxygenation (HDO), and hydrogenation (HYD). It is well accepted that the active component of hydrotreatment catalysts comprises nanosized MoS_2 particles with cobalt or nickel atoms decorating their edges and corners;[16] these particles form the Co(Ni)-Mo-S phase. Two types of the Co(Ni)-Mo-S phase were described in the literature.[17-19] Type I, characterised by incomplete sulphidation, is formed after low-temperature sulphidation; it has a lower degree of hydrodesulphurisation (HDS) activity than type II, which is formed after high-temperature sulphidation and is fully sulphided.

In our previous study,[20] it was found that the CoO-MoO_3/γ-Al_2O_3 catalyst sulphided at 400 °C exhibited the highest catalytic activity because it possessed the most CoMoS type I structures. A CoMoS type I structure, which is formed at low temperature, can transform into CoMoS type II when the sulphidation temperature increases. What's more, CoMoS type II structure did not favor sulphur-resistant methanation reaction.

Although there are ample studies in the literature on the application of sulphided Ni-Mo catalysts in hydrotreating especially HDN reactions, no studies have focused on their application to sulphur-resistant methanation. In this work, we attempted to investigate the effects of the sulphidation temperature on the catalytic performance of NiO-MoO_3/Al_2O_3 for sulphur-resistant methanation from syngas. The catalysts were sulphided at a range of temperatures; characterized by BET, TPS, XRD, RS, XPS and TEM; and evaluated in a fixed-bed reactor. In addition, the properties of as-prepared catalysts were further investigated, in order to understand the correlations between structure and activity.

Experimental

Catalyst preparation

A commercial γ-Al_2O_3 powder (Qianye Non-metallic Material Co. Ltd., China) was used as the catalyst support. The monometallic NiO/γ-Al_2O_3 and MoO_3/γ-Al_2O_3 catalysts were prepared by the incipient wetness impregnation method. The bimetallic NiO-MoO_3/γ-Al_2O_3 catalysts were prepared by co-impregnation method. The γ-Al_2O_3 support was impregnated by aqueous solution of nickel nitrate hexahydrate ($Ni(NO_3)_2{\cdot}6H_2O$) (Kemiou chemical reagent Co. Ltd., Tianjin), aqueous solution of heptamolybdate tetrahydrate ($(NH_4)_6Mo_7O_{24}{\cdot}4H_2O$) (Kemiou Chemical Reagent Co. Ltd., Tianjin), mixed aqueous solution of heptamolybdate tetrahydrate and nickel nitrate hexahydrate, respectively. The samples were dried at room temperature for 48 h, subsequently dried at 120 °C for 4 h and calcined at 600 °C for 5 h with a heating rate of 5 °C/min. According to our previous work,[21, 22] the amount of Ni oxides and Mo oxides in

the catalyst were approximately 5.0 wt% and 25.0 wt% for three catalysts, respectively. It was found that the exact loadings of Ni and Mo measured by ICP (Varian-MPX) in the final catalyst were consistent with the amount estimated.

Catalyst characterisation

N_2 adsorption and desorption isotherm of the catalysts was performed at -196 °C on a Tristar-3000 apparatus (Micro-meritics, United States) to obtain the textural properties of the catalysts (i.e., specific surface areas and pore volumes). Each sample was degassed at 300 °C for 4 h before the adsorption measurement. The X-ray diffraction (XRD) pattern was obtained using a Rigaku D/max-2500 X-ray diffractometer (40 kV, 200 mA) with a Ni-filtered Cu-Kα radiation (λ=1.54056 Å). The scan speed was 5°/min with a scanning angle ranged from 5° to 90°. The phases were identified by comparison to powder diffraction data from the Joint Committee on Powder Diffraction Standards (JCPDS). The Laser Raman spectra were obtained using an InVia-Reflex (Renishaw, England) laser Raman spectrometer, integrated with highly sensitive, research-grade microscopes. The 532 nm emission line from the Ar^+ ion laser (Spectra Physics) was employed for the incident light, and this 6 mW beam was focused on the samples using the system microscope. The laser beam intensity and the spectrum slit width were 8 mW and 25μm, respectively. The samples were pressed into pellets for the measurements. X-ray photoelectron spectroscopy (XPS) analysis of all catalyst samples was performed using a PHI-1600 ESCA XPS system with monochromatic Mg-K radiation and a chamber pressure of 2×10^{-10} Torr. The binding energies were calibrated to the C^{1s} line at 284.6 eV. The peak areas were measured using a planimetric technique that assumed a linear baseline. The morphology and structure of the catalysts were characterised via a Tecnai G^2F20 (200 kV) high-resolution transmission electron microscope (TEM) (FEI, Holland), which has a maximum resolution of 0.15 nm/200 kV. For analysis, each sample was ultrasonically dispersed in ethanol and then deposited onto a copper grid.

Sample sulphidation for characterisation

Sulphidation experiments were performed in a quartz tube reactor (inner diameter 10 mm and length 500 mm), similar to previous studies.[20, 23] In each experiment, the NiO-MoO_3/γ-Al_2O_3 catalyst (3mL) with particle diameter between 0.43 mm to 0.85 mm was sandwiched between quartz fibres in the middle of the reactor and subjected to 3 vol% H_2S in H_2 (Dalian Date Gas Co. Ltd., China) at a flow rate of 100 mL/min. For each sulphidation process, the catalysts were heated to the desired temperature at a rate of 3 °C/min and maintained at that temperature for 4 h. Afterward, catalysts were cooled down to room temperature under nitrogen atmosphere and stored in a vacuum dryer.

Evaluation of catalytic activity

Catalytic performance was evaluated using a continuous-flow, fixed-bed reactor. The tubular, stainless steel reactor had an inner diameter of 12 mm and a length of 700 mm. The experimental apparatus had been described in detail in our previous study.[24] Prior to the reaction, the catalyst (3 mL) was sulphided in situ at 400 °C for about 4 h in a 3 vol% H_2S/H_2 flow at atmospheric pressure. The following conditions were applied to evaluate the catalytic activity: syngas (H_2/CO = 1.0) containing 0.12 vol% H_2S and 20 vol% N_2, a gas hourly space velocity of 5000 h^{-1}, a temperature of 550 °C and a pressure of 3.0 MPa. The outlet gases were online analysed by using an Agilent 7890A GC system equipped with two sets of TCD and one FID. External standard method was used to calibrate the GC results getting the composition of each component in the outlet gases. The catalytic activity was represented by conversion of CO and yield of CH_4, which were obtained after 20 h reaction. The CO conversion, the CH_4 selectivity, the CO_2 selectivity and CH_4 yield were calculated using the following equations as previous work shown[25]:

$$X_{CO}=\frac{n(CO)_{in}-n(CO)_{out}}{n(CO)_{in}}*100\% \quad (4) \qquad S_{CH4}=\frac{n(CH_4)_{out}}{n(CO)_{in}-n(CO)_{out}}*100\% \quad (5)$$

$$S_{CO2}=\frac{n(CO_2)_{out}}{n(CO)_{in}-n(CO)_{out}}*100\% \quad (6) \qquad S_{C2H6}=\frac{2n(C_2H_6)_{out}}{n(CO)_{in}-n(CO)_{out}}*100\% \quad (7)$$

$$Y_{CH4} = X_{CO} * S_{CH4} * 100\% \quad (8)$$

Results and discussions

Effect of the sulphidation temperature on the textural, structural properties of NiO-MoO_3/γ-Al_2O_3 catalysts

The BET surface area, pore volumes and the average pore diameter of the NiO-MoO_3/γ-Al_2O_3 catalyst and its sulphided samples were given in Table 1. Obviously, the BET surface area and pore volume of the sulphided samples were generally smaller than those of non-sulphided sample. The average pore sizes of the sulphided samples were mainly larger than those of the non-sulphided sample (except the sample sulphided at 400 °C). It was found that the BET specific surface area slightly decreased, while the particle size increased upon the sulphidation temperature. The reason could be caused by blockage of the pores and the formation of bulk and crystalline MoS_2 with the increase of sulphidation temperature. It could thus be deduced that the BET surface area generally decreased with increasing particle size. Hysteresis loops, presented in Fig. 1, could be obviously observed for the NiO-MoO_3/γ-Al_2O_3 catalyst and its sulphided samples. These hysteresis loops are in typical IV type with H3 shape according to the IUPAC classification, which reveals slit-shaped mesoporous structure. Furthermore, the hysteresis loops for all sulphided samples were quite similar to one another, which indicated that the structure of the samples was not destroyed during the sulphidation process.

Table 1 The textural properties of NiO-MoO_3/γ-Al_2O_3 catalyst and sulphided samples at different temperatures

ST(°C)[a]	BET[b] (m^2/g)	PV[c] (cm^3/g)	PD[d] (nm)
-	174	0.354	6.62
200	171	0.321	6.72
300	168	0.302	6.62
400	163	0.312	6.85
500	122	0.301	7.23
600	78	0.266	8.46

[a] Sulphidation temperature; [b] BET surface area; [c] Pore volume; [d] Pore diameter.

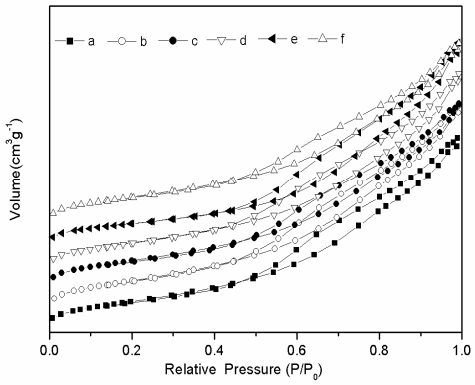

Fig. 1 N_2 isothermal adsorption and desorption profiles over NiO-MoO_3/γ-Al_2O_3 catalysts sulphided at different temperatures: (a) non-sulphided, (b) 200 °C, (c) 300 °C, (d) 400 °C, (e) 500 °C and (f) 600 °C.

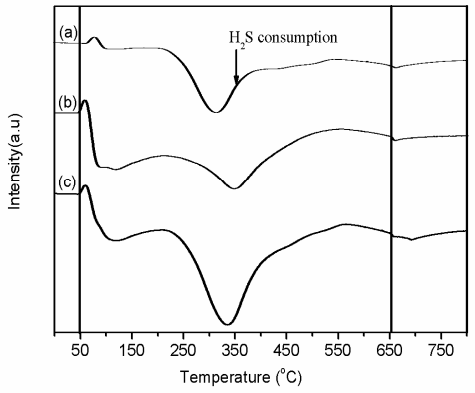

Fig. 2 TPS profiles of (a) NiO/γ-Al_2O_3 catalyst, (b) MoO_3/γ-Al_2O_3, catalyst and (c) NiO-MoO_3/γ-Al_2O_3 catalyst.

To understand the sulphidation conditions, the sulphidation behaviours of the NiO/γ-Al_2O_3, MoO_3/γ-Al_2O_3 and NiO-MoO_3/γ-Al_2O_3 catalysts were investigated via TPS techniques. Fig. 2 presented the TPS profiles of these catalysts. As shown in Fig. 2 (a), there were two H_2S consumption regions in the hydrogen sulphide consumption profile of the NiO/γ-Al_2O_3 sample. This result meant that the Ni species would be sulphide until the sulphidation temperature was above ~320 °C. Bastow et al.[21] reported the Ni_3S_2 phase appeared firstly, then it changed to the NiS phase gradually with increasing

sulphidation temperature. This was consistent with the second weak H_2S consumption region, i.e., the Ni_3S_2 phase was gradually sulphided to NiS as the sulphidation temperature rose from 550 °C to 700 °C. As shown in Fig. 2 (b), there were three H_2S consumption regions for the MoO_3/γ-Al_2O_3 catalyst. The first region, below 200 °C, was associated with a simple O-S exchange to form MoO_xS_y species.[26, 27] The second H_2S consumption region (250 - 500 °C) was attributed to further sulphidation of MoO_xS_y to form a MoS_2 structure. And the last region (> 550 °C) arose from the sulphidation of a Mo-O-Al structure which indicated the MoO_3/γ-Al_2O_3 catalyst was completely sulphide.[28] The TPS profile of the NiO-MoO_3/γ-Al_2O_3 catalyst was displayed in Fig. 2 (c). Three H_2S consumption regions could be observed clearly in the TPS profile of the NiO-MoO_3/γ-Al_2O_3 catalyst, including H_2S consumption regions of the NiO/γ-Al_2O_3 and MoO_3/γ-Al_2O_3 catalysts during sulphidation. The sulphided regions were broader than those of the NiO/γ-Al_2O_3 and MoO_3/γ-Al_2O_3 catalyst. This result could be attributed to the sulphidation of the Ni and Mo species in the catalyst. As reported in the literature,[29] catalyst sulphidation included in three main stages: (1) initial exchange of surface oxygen for sulphur; (2) reduction of molybdenum accompanied by the release of hydrogen sulphide; and (3) slow sulphiding of the remaining oxygen. The results of the TPS profiles in this study were in good agreement the sulphiding stages described above.

Fig.3 presented the X-ray diffraction patterns of the NiO-MoO_3/γ-Al_2O_3 samples sulphided at 200, 300, 400, 500, and 600 °C. For comparison, the XRD pattern of the non-sulphided sample was also included. And three primary γ-Al_2O_3 diffraction peaks were detected at 2θ= 37.5°, 45.7°, and 66.6°, which were also found in the XRD spectra of the sulphided samples. There was an additional feature observed at 2θ=26.7°, which might be due to β-$NiMoO_4$ (tetrahedral Mo coordination).[30] The formation of these crystallites, which was caused by the interaction between the Ni and Mo species, were highly dispersed on the support. In addition, no diffraction peaks corresponding to crystallographic MoO_3 or nickel oxides were detected in the non-sulphided sample, which meant that molybdenum oxide and nickel oxide totally dispersed on the γ-Al_2O_3 support.[24, 31] When the catalyst was sulphided at 200 °C, there were no distinct diffraction peaks for the MoS_2 phase, indicating no MoS_2 crystal formation, i.e., the catalyst was not sulphided at 200 °C. Instead, weak diffraction peaks with 2θ at around 33° and 59° characteristic for the (100) and (110) planes of the hexagonal phase of MoS_2 [PDF 37-1492] occurred after sulphidation at 300 °C. This result meant that the oxidic precursor began being sulphided at 300 °C, in accordance with the results from TPS. Furthermore, the intensity of these diffraction lines enhanced with the increase of sulphidation temperature, demonstrating that large MoS_2 crystallites were formed as the sulphidation temperature increased. Moreover, a $NiMoS_4$ phase was observed at 2θ=38° for samples sulphided at temperature of 400 °C or above.[32] It could be deduced that NiMoS structure was formed when the sulphidation temperature was 400 °C or above.

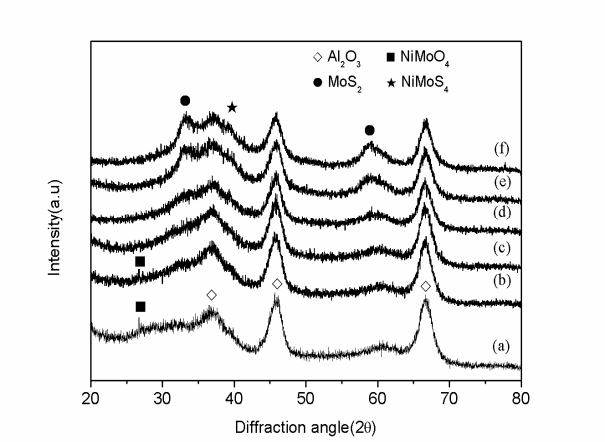

Fig. 3 X-ray diffraction patterns of NiO-MoO_3/γ-Al_2O_3 sulphided at different temperatures: (a) non-sulphided, (b) 200 °C, (c) 300 °C, (d) 400 °C, (e) 500 °C and (f) 600 °C.

In complementary with the XRD spectra, the laser Raman spectra of the NiO-MoO_3/γ-Al_2O_3 catalyst and samples sulphided at different teperatures were illustrated in Fig. 4. The Raman spectrum of the NiO-MoO_3/γ-Al_2O_3 catalyst (non-sulphided) revealed a

dominant asymmetric feature at 961 cm^{-1}, which was attributed to the β-$NiMoO_4$ phases[33] (Fig. 4(a)), and was in agreement with the XRD results in Fig. 3. In addition, the Raman band at ~925 cm^{-1}, ~359 cm^{-1}, ~579 cm^{-1} and 227 cm^{-1} were associated with the symmetric stretching and bending modes of the terminal Mo=O bond, and the Mo-O-Mo symmetric stretch and deformation modes of the amorphous octahedrally coordinated Mo^{6+}(O) species, respectively.[34-37] The intensity of these bands decreased with the increase of sulphidation temperature. With respect to the sulphided samples, a dominant peak at 961 cm^{-1}, which was attributed to the $NiMoO_4$ phases, was not found. This result was likely caused by the sulphidation of the $NiMoO_4$ phases during the sulphidation process. Meanwhile, the Raman band at 383 cm^{-1}, 408 cm^{-1} and 281 cm^{-1} are ascribable to the MoS_2 phases.[38, 39] Additionally, the intensity of these bands gradually strengthened with the increase of sulphidation temperature. As the sulphidation temperature rose, there were increasingly more MoS_2 phases formed. All of these phenomena were in agreement with XRD analysis. Notably, the Raman bands at 848 cm^{-1} and 1002 cm^{-1}, corresponding to the MoO_3,[40] were also found in these sulphided samples and not found in the non-sulphided samples. In fact, the Raman bands at 848 cm^{-1} and 1002 cm^{-1} were overlapped by the dominant asymmetric feature at 961 cm^{-1}. It was probable that exposure of the samples to air following sulphidation could cause partial sulphided samples re-oxidation and thereby made it easy to the presence of MoO_3.

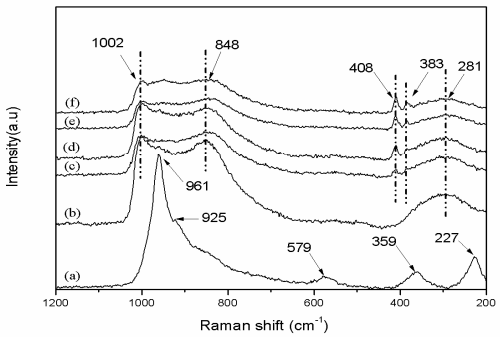

Fig. 4 Laser Raman spectra of NiO-MoO_3/γ-Al_2O_3 sulphided at different temperatures: (a) non-sulphided, (b) 200 °C, (c) 300 °C, (d) 400 °C, (e) 500 °C and (f) 600 °C.

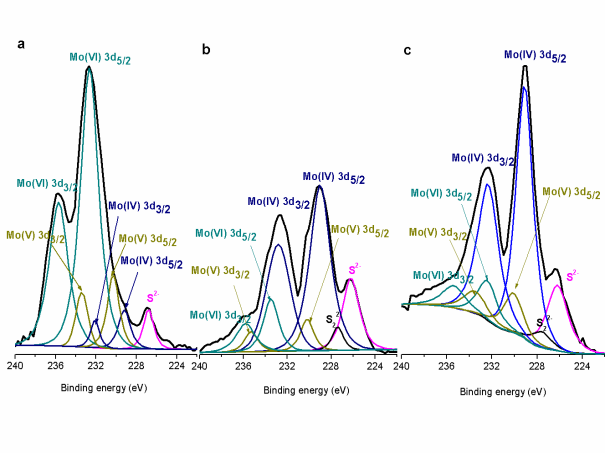

Fig. 5 Deconvolution of XPS Mo 3d spectra of the catalysts sulphided at different temperatures: 200 °C (a), 400 °C (b), 600 °C (c).

In addition, XPS experiments allowed evaluating the part of Mo and Ni involved in the different phases encountered on the catalysts surface. For simplicity, the deconvolution of Mo 3d and Ni $2p_{3/2}$ spectra for only catalysts sulphided at three representative temperatures (200 °C, 400 °C and 600 °C) were reported (Fig. 5 and Fig. 6). The deconvolution of Mo 3d spectra was well documented.[41-44] Molybdenum could exist as disulphide MoS_2 (Mo^{IV}), the doublet was located at 229.0 ± 0.1 eV (Mo^{IV} $3d_{5/2}$) and 232.1 ± 0.1 eV (Mo^{IV} $3d_{3/2}$). The existence of a Mo oxide phase (MoO_x or $NiMoO_4$, Mo^{VI}) was elucidated by two contributions located at 232.2 ± 0.1eV (Mo^{VI} $3d_{5/2}$) and 235.3 ± 0.1 eV (Mo^{VI} $3d_{3/2}$). The last phase was, according to the literature, an intermediate state Mo oxysulphide speaces (MoO_xS_y, Mo^{V}). For this species the doublet appeared at 230.2 ± 0.1 eV (Mo^{V} $3d_{5/2}$) and 233.4 ± 0.1eV (Mo^{V} $3d_{3/2}$). In addition, in the same part of the spectra two bands appeared corresponding to the S 2s contributions decomposed in two different sulphur species (226.0 ± 0.1 eV and 227.6 ± 0.2 eV) which was attributed to S^{2-} (MoS_2) and S_2^{2-} (MoO_xS_y) species, respectively.[45] These sulphur species must be subtracted from the total spectrum of Mo 3d. Proper deconvolution of the registered peaks provided the data summarized in Table 2. There was a significant influence of the sulphidation temperature on the distribution of Mo species. The highest atomic percentage of (Mo^{IV}) sulphide phase and the lowest atomic percentages of (Mo^{V}, Mo^{VI}) phases were obtained for the NiO-MoO_3/γ-Al_2O_3 catalyst. This

confirmed that Mo contained in the catalyst was well sulphided at 600 °C, i.e., the sulphidation degree of NiO-MoO_3/γ-Al_2O_3 was correlated to the sulphidation temperature.

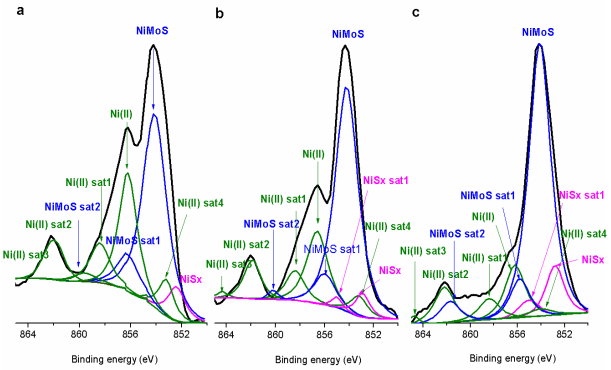

Fig. 6 Deconvolution of XPS Ni $2p_{3/2}$ spectrum of the catalysts sulphided at different temperatures: 200 °C (a), 400 °C (b), 600 °C (c).

Table 2 XPS parameters of the different contributions Mo 3d obtained for NiO-MoO_3/γ-Al_2O_3 sulphided at different temperatures

ST(°C)	Mo^{IV}		Mo^{V}		Mo^{VI}	
	BE(eV)	%atom.	BE(eV)	%atom.	BE(eV)	%atom.
200	229.2	22.3	230.2	33.1	232.4	44.6
400	229.1	56.5	230.3	24.3	232.5	19.2
600	229.3	84.1	230.2	10.3	232.4	5.6

Table 3 XPS parameters of the different contributions Ni $2p_{3/2}$ obtained for NiO-MoO_3/γ-Al_2O_3 sulphided at different temperatures

ST(°C)	NiMoS phase		NiSx phase		Ni^{II} phase	
	BE(eV)	%atom.	BE(eV)	%atom.	BE(eV)	%atom.
200	853.5	46.6	852.9	15.9.	855.8	37.5
400	853.4	67.4	852.5	14.5	855.9	18.1
600	853.5	80.8	852.8	11.4	855.4	7.8

Respecting the analysis of surface Ni species, the Ni 2p envelope was decomposed by considering three major contributions corresponding to NiS_x sulphided phase (which could arise from Ni_2S_3, Ni_9S_8 or NiS, with binding energy between 852.9 and 853.8 eV), to oxidic nickel on the Al_2O_3 carrier (binding energy of 856.9 eV) and the NiMoS phase (with binding energy between 853.5 and 854 eV).[46, 47] The relative quantities of Ni species (Ni^{II} oxide, NiS_x, and NiMoS) depending on the nature of the support were reported in Table 3. A higher proportion of NiMoS phase was obtained on NiO-MoO_3/γ-Al_2O_3 sulphided at 600 °C, in which 80.8% of the nickel atoms were engaged. This value was higher than those obtained for catalysts sulphided at the low temperature, demonstrating that $NiMoO_4$ phases were transformed into $NiMoS_4$ upon sulphidation.

Table 4 Surface XPS atomic ratios of NiO-MoO_3/γ-Al_2O_3 catalysts sulphided at different temperatures

ST(°C)	S/(Ni+Mo)	Mo/Al	Ni/Al	S/Al
200	0.800	0.127	0.0403	0.134
400	1.80	0.101	0.0380	0.227
600	2.05	0.0974	0.0252	0.279

The surface XPS atomic ratios of the sulphided samples were also compiled in Table 4. For sulphided catalysts, the Mo/Al ratios decreased markedly with the increase of sulphidation temperature. Meanwhile, a similar trend was observed for the Ni/Al ratios. The drastic decrease in both Mo/Al and Ni/Al ratios upon sulphidation suggested the formation of large sulphide particles at the surface of aluminium oxide. The S/Al and S/(Ni+Mo) ratios increased substantially, however, as the sulphidation temperature rose, thus indicating that the degree of sulphidation depends on, to a large extent, the temperature. Furthermore, catalysts sulphided at 600 °C had higher S/(Ni+Mo) and S/Al ratios, which indicated a larger degree of sulphidation of these catalysts.

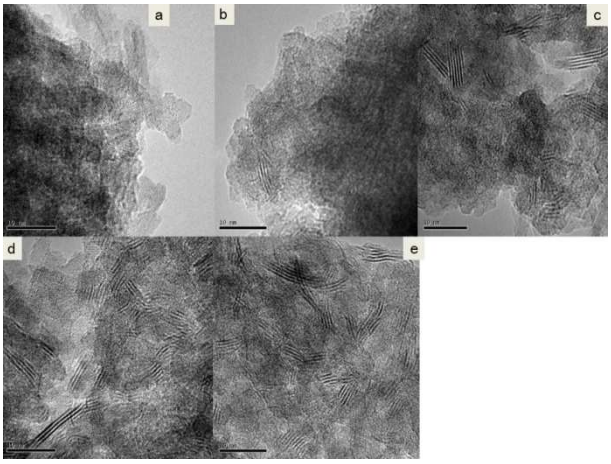

Fig. 7 TEM images of NiO-MoO_3/γ-Al_2O_3 catalyst sulphided at (a) 200 °C, (b)300 °C, (c)400 °C, (d) 500 °C and (e) 600 °C.

The HRTEM images of catalysts sulphided at different temperatures were showed in Fig.7. It gave information about the morphology of MoS_2, the distribution of slab length (L) and the number of fringes (N). Fig. 7 presented pictures of typical crystallite of NiO-MoO_3/γ-Al_2O_3 phase sulphided at differernt

temperatures. Obviously, no distinct stacked MoS_2 crystals were found in the catalysts sulphided at or below 300 °C, which was in good agreement with the results of XRD and Raman spectroscopy. Nanosized spot-like entities were found to exist in these catalysts, and these entities were assigned to non-crystalline Mo oxysulfide particles.[48] These entities were barely found in the catalysts sulphided above 300 °C, which were attributed to the high temperature sulphidation of these entities. With the increase of sulphidation temperature, the micrographs consistently displayed increasingly more stripes that represented MoS_2 phase. There were abundant black thread-like fringes corresponding to the MoS_2 slabs with different stack height and length evenly distributed on the surface of Al_2O_3. What's more, the stacking number and length of stacked MoS_2 crystals were presented in Table 5 by statistical analysis of the HRTEM images. For the catalyst sulphided at 300 °C the average stack length was 2.14 nm and the average stacking number was 1.73 layers. With a further increase in the sulphidation temperature, larger MoS_2 particles were predominantly formed as seen in case of catalysts sulphided at higher temperatures. The stacking number and length of stacked MoS_2 crystallites increased with increasing sulphidation temperature. Meanwhile, HRTEM showed that the MoS_2 slabs for those catalysts sulphided at high temperature were larger and more stacked than those at low temperature, which suggested that less Mo_{edge}^{IV} active sites were available on the catalyst surface.[43] The results of TEM demonstrated that the degree of sulphidation MoO_3 strengthened and large MoS_2 phase crystallites formed, which were in good accordance with XRD and Raman results.

Table 5 Average slabs length and stacking degree (as determined by HRTEM) of MoS_2 phase crystallites present the NiO-MoO_3/γ-Al_2O_3 catalyst sulphided at different temperatures

ST(°C)	Average length L (nm)	Average stacking number
200	-	-
300	2.14	1.73
400	2.66	1.96
500	3.58	3.23
600	4.17	3.65

The sulphidation temperature was found to have a pronounced influence on both textural and structural properties of the NiO-MoO_3/γ-Al_2O_3 catalysts. Furthermore, based on the results of TPS, XRD, Raman spectroscopy and TEM, we could divide the temperature range into two zones and separately discuss the variations observed in the properties of the resulting sulphides.

(I) Sulphidation temperature below 400 °C: In this region, it's not observed any significant influence on the texture of the NiO-MoO_3/γ-Al_2O_3 sulphides. Based on the results of the N_2 adsorption-desorption (Table 1 and Fig. 1), the BET surface, pore volumes and average pore sizes were basically the same. As previously reported in the literature,[49, 50] the β-$NiMoO_4$, which was more easily converted into NiMoS active sites during the sulphidation process, was the precursor of the NiMoS structure. The XRD and RS results elucidated that $NiMoO_4$ species were existed in the NiO-MoO_3/γ-Al_2O_3 catalyst. Therefore, the Ni species and Mo species could form a NiMoS structure during the sulphidation process. The NiMoS structure was formed by the Ni atom located on the edge of MoS_2 crystal.[16] In other words, the formation of MoS_2 crystal was a prerequisite for the formation of NiMoS structure. At low sulphide temperature, no NiMoS phase formed until the MoS_2 particles were formed. The XRD and RS results demonstrated that the formation of MoS_2 occurred when the sulphidation temperature was 300 °C. The TEM results indicated, however, that MoS_2 crystals could be visible in the catalyst until the sulphidation temperature reached 400 °C. Herein, it could be concluded that the NiO-MoO_3/γ-Al_2O_3 catalyst was only partial sulphidation at 300 °C.

(II) Sulphidation temperature in the range of 400 - 600 °C: A drastic decrease in the specific surface area accompanied by a significant increase of the size of the MoS_2 particles was observed in this temperature range (Table 1). XRD, Raman, and XPS analyses demonstrated that the intensity of sulphidation progressively enhanced with the increase of sulphidation temperature. Previous reports in the literature reported that the type of NiMoS structures could be divided into NiMoS type I and NiMoS type II, which formed incomplete sulphidation and fully sulphide, respectively.[28]

Generally speaking, this demonstrated that the formation of NiMoS type depended on the sulphidation temperature. According to the results of XPS, NiMoS phases were formed during the sulphidation process. Higher proportion of NiMoS phase was obtained at higher sulphidation temperature. In addition, TEM presented MoS_2 slabs with significantly higher stacking and an average higher length as the sulphidation temperature rose. By combination of XPS quantification and HRTEM micrographs, there were more and more stripes represented MoS_2 with the temperature increased from 400 to 600 °C. This strongly suggested that NiMoS type II were formed at the high sulphidation temperatures. It could be deduced that the NiMoS phase could be changed with the sulphidation temperature.

Effect of the sulphidation temperature on catalytic activity

The activities of the NiO-MoO_3/γ-Al_2O_3 catalysts sulphided at different temperatures were tested, and the results were showed in Fig. 8. For comparison, the activity of the non-sulphided NiO-MoO_3/γ-Al_2O_3 catalyst was also given. Meanwhile, to be remarkable, even though the non-sulphided catalyst showed a better stability than other catalysts, it exhibited minimum CO conversion among these catalysts. This result meant that the NiO-MoO_3/γ-Al_2O_3 oxidic precursor did not possess better methanation activity, and that sulphidation played a vital role in determining the catalytic performance of such catalyst as reported in the literature.[10] When the sulphidation temperature was at or lower than 400 °C, the catalytic activities was greatly improved with increasing of sulphidation temperature. The XRD and RS results showed that the $NiMoO_4$ species was sulphided until the sulphidation temperature was above 300 °C. It illustrated that appropriately sulphided $NiMoO_4$ species exhibited much better catalytic activity, which can be due to the formation of NiMoS structure during the catalyst sulphidation. When the sulphidation temperature was above 400 °C, the catalytic activity of NiO-MoO_3/γ-Al_2O_3 decreased with increasing of sulphidation temperature. What's more, the CH_4 yield had the same trend as well as the CO conversion and reached the maximum value at the sulfidation temperature of 400°C. However, the CO conversion gradually decreased as the reaction progress. The reason might be due to the aggregation of MoS_2 nanoparticles and the formation of MoS_2 crystallites during the methanation reaction in high temperature. As shown in Fig. 8, the selectivity of CH_4, CO_2 and C_2H_6 on the several catalysts were more or less the same (the value changed less than 3%), i.e., the calcination temperature had no significant effect on the selectivity. In general, the NiO-MoO_3/γ-Al_2O_3 catalyst sulphided at 400 °C exhibited the best catalytic activities for sulphur-resistant methanation among others, involving in the highest CO conversion and CH_4 yield.

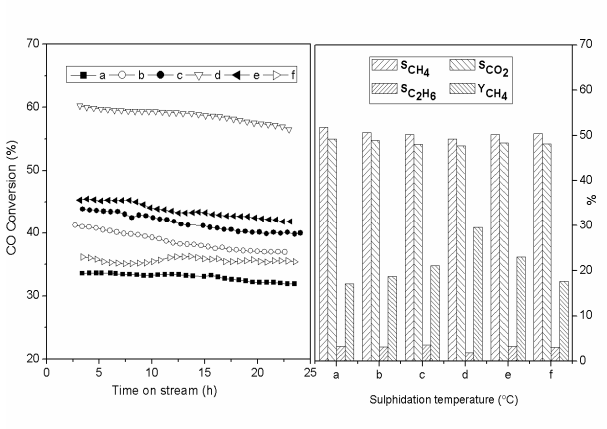

Fig. 8 CO conversion and selectivity of NiO-MoO_3/γ-Al_2O_3 catalysts sulphided at different temperatures: (a) non-sulphided, (b) 200 °C, (c) 300 °C, (d) 400 °C, (e) 500 °C and (f) 600 °C.

As discussed above, the BET specific surface areas of the catalysts decreased with increasing sulphidation temperature. The decrease in BET specific surface is one of the factors leading to the decrease in catalytic activity, but not the key one. Generally, in the NiMoS catalyst system, Ni atoms were incorporated into Mo vacancies at the edge locations of the MoS_2 crystallites. Only the NiMoS structure, which was formed by interactions between the edge atoms of MoS_2 and Ni atoms, had been reported to show the catalytic activity, while Mo sites on the basal plane area were almost inactive.[51] Moreover, the TEM results illuminated that the stacking number and the length of stacked MoS_2 distinctly increased when the catalyst was sulphided at higher than 400 °C. The formation of MoS_2

crystals decreased the edge atoms of MoS_2 where Ni atoms were located. The quantification of the active Mo^{IV} sites was achieved by XPS and the morphology of MoS_2 slabs were examined by TEM. By combination of XPS quantification, the MoS_2 slabs of catalysts sulphided at high temperature are longer, the stacking is higher, and apparent Mo_{edge}^{IV} active sites are relegated. This strongly suggested that NiMoS type II were formed at the high sulphidation temperatures. Presumably, the active structure changed from NiMoS type I to NiMoS type II with increasing sulphidation temperature. Therefore, the deterioration in the catalytic activity of NiO-MoO_3/γ-Al_2O_3 sulphidation at higher temperatures could be speculated as the following reasons: (1) a decrease in the BET specific surface area; (2) an increase in the amount of stacked MoS_2 crystals accompanied a decrease in the Mo_{edge}^{IV} active sites; (3) an increasingly progressive transformation of the NiMoS phase with the increase of sulphidation temperature.

In HDS reactions, the NiMoS type II structure that was formed at a high sulphidation temperature of 600 °C exhibited better catalytic activity than the NiMoS type I structure that formed at a sulphidation temperature of 400 °C. Nevertheless, in the sulphur-resistant methanation system, the catalyst sulphided at 400 °C had a higher catalytic activity than the catalyst sulphided at 600 °C. This result suggested that the active reaction centres for HDS and methanation were different. In addition, the combined results of XRD, RS, and TEM revealed that NiMoS type II formed at 600 °C with numerous crystalline MoS_2 species. The crystalline MoS_2 structure showed lower methanation activity. As a result, these phenomena indicated that the formation of a NiMoS type II structure did not favour sulphur-resistant methanation reaction, similar to the CoMoS type II structure.

In agreement with a previous study[18], no matter which promoter (cobalt or nickel) was used in the MoS_2-based catalysts for methanation, the Co(Ni)-Mo-S type I structure exhibited higher catalytic activity, and formation of a Co(Ni)-Mo-S type II structure did not favour the sulphur-resistant methanation reaction. However, this result was totally different from the HDS reactions in which the Co(Ni)-Mo-S type II structure formed at high sulphidation temperatures displayed catalytic activity approximately twice as high as the Co(Ni)-Mo-S type I structure.

Conclusions

The effect of sulphidation temperature on the catalytic performance of NiO-MoO_3/γ-Al_2O_3 catalyst toward sulphur-resistant methanation was investigated in this study. The present work led to the following main conclusions: (1) the NiO-MoO_3/γ-Al_2O_3 catalyst possessed higher catalytic activity after the sulphidation of $NiMoO_4$, and the best sulphidation temperature of NiO-MoO_3/γ-Al_2O_3 catalyst was around 400 °C. (2) When the sulphidation temperature was higher than 400 °C, the catalytic activity of NiO-MoO_3/γ-Al_2O_3 catalyst decreased with increasing of sulphidation temperature. This was attribute to the transformation of NiMoS phase progressively increases with sulphidation temperature and the increase of stacked MoS_2 crystals accompanied less Mo_{edge}^{IV} active sites; (3) the formation of NiMoS type II structure did not display good performance for the sulphur-resistant methanation, because the formation of this species accompanied crystalline MoS_2 in catalysts, which showed lower methanation activity.

Notes and references

* Key Laboratory for Green Chemical Technology of Ministry of Education, School of Chemical Engineering and Technology, Tianjin University, Tianjin 300072, China. E-mail: wangbw@tju.edu.cn

1. A. L. Kustov, A. M. Frey, K. E. Larsen, T. Johannessen, J. K. Nørskov and C. H. Christensen, *Appl. Catal., A*, 2007, 320, 98-104.
2. I. Chen and D. W. Shiue, *Ind. Eng. Chem. Res.*, 1988, 27, 1391-1396.
3. A. V. Pashigreva, G. A. Bukhtiyarova, O. V. Klimov, Y. A. Chesalov, G. S. Litvak and A. S. Noskov, *Catal. Today*, 2010, 149, 19-27.
4. J. Happel, M. Yoshikiyo, F. S. Yin, M. Otarod, H. Y. Cheh, M. A. Hnatow, L. Bajars, H. S. Meyer and I. Chen, *Ind. Eng. Chem. Prod. Res*, 1986, 25, 214-219.
5. Y. Okamoto, S. y. Ishihara, M. Kawano, M. Satoh and T. Kubota, *J. Catal.*, 2003, 217, 12-22.
6. P. Afanasiev, *J. Catal.*, 2010, 269, 269-280.
7. M. Nagai and K. Matsuda, *J. Catal.*, 2006, 238, 489-496.
8. G. Z. Bian, F. Li, Y. L. Fu and K. Fujimoto, *Appl. Catal., A*, 1998, 170, 255-268.

9. P. Arnoldy, J. A. M. van den Heijkant, G. D. de Bok and J. A. Moulijn, *J. Catal.*, 1985, 92, 35-55.
10. X. R. Shi , J. G. Wang and K. Hermann, *J. Phys. Chem. C*, 2010, 114, 6791-6801.
11. M. de Boer, A. J. van Dillen, D. C. Koningsberger and J. W. Geus, *J. Phys. Chem.*, 1994, 98, 7862-7870.
12. P. J. Mangnus, E. K. Poels and J. A. Moulijn, *Ind. Eng. Chem. Res.*, 1993, 32, 1818-1821.
13. Y. E. Licea, S. L. Amaya, A. Echavarría, J. Bettini, J. G. Eon, L. A. Palacio and A. C. Faro, *Catalysis Sci Tech*, 2014, 4, 1227.
14. I. V. Deliy, E. N. Vlasova, A. L. Nuzhdin, E. Y. Gerasimov and G. A. Bukhtiyarova, *RSC Adv.*, 2014, 4, 2242.
15. C. Bouvier, Y. Romero, F. Richard and S. Brunet, *Green Chem.*, 2011, 13, 2441-2451.
16. N. Y. Topsøe and H. Topsøe, *J. Catal.*, 1983, 84, 386-401.
17. H. Topsøe and B. S. Clausen, *Catal. Rev. Sci., Eng.*, 1984, 26, 395-420.
18. H. Topsøe and B. S. Clausen, *Appl. Catal.*, 1986, 25, 273-293.
19. H. Topsøe, B. S. Clausen, R. Candia, C. Wivel and S. Mørup, *J. Catal.*, 1981, 68, 433-452.
20. M. H. Jiang, B. W. Wang, Y. Q. Yao, Z. H. Li, X. B. Ma, S. D. Qin and Q. Sun, *Catalysis Sci. Tech.*, 2013, 3, 2793-2800.
21. B. Wang, G. Ding, Y. Shang, J. Lv, H. Wang, E. Wang, Z. Li, X. Ma, S. Qin and Q. Sun, *Appl. Catal., A*, 2012, 431-432, 144-150.
22. M. Jiang, B. Wang, Y. Yao, Z. Li, X. Ma, S. Qin and Q. Sun, *Catalysis Sci. Tech.*, 2013, 3, 2793.
23. M. H. Jiang, B. W. Wang, J. Lv, H. Y. Wang, Z. H. Li, X. B. Ma, S. D. Qin and Q. Sun, *Appl. Catal., A*, 2013, 466, 224-232.
24. B. W. Wang, G. Z. Ding, Y. G. Shang, J. Lv, H. Y. Wang, E. D. Wang, Z. H. Li, X. B. Ma, S. D. Qin and Q. Sun, *Appl. Catal., A*, 2012, 431-432, 144-150.
25. M. Jiang, B. Wang, Y. Yao, H. Wang, Z. Li, X. Ma, S. Qin and Q. Sun, *Appl. Catal., A*, 2014, 469, 89-97.
26. T. F. Hayden and J. A. Dumesic, *J. Catal.*, 1987, 103, 366-384.
27. J. C. Muijsers, T. Weber, R. M. Vanhardeveld, H. W. Zandbergen and J. W. Niemantsverdriet, *J. Catal.*, 1995, 157, 698-705.
28. J. A. R. van Veen, H. A. Colijn, P. A. J. M. Hendriks and A. J. van Welsenes, *Fuel Process. Technol.*, 1993, 35, 137-157.
29. P. Zeuthen, P. Blom, B. Muegge and F. E. Massoth, *Appl. Catal.*, 1991, 68, 117-130.
30. F. J. Maldonado-Hódar, L. M. P. Madeira and M. F. Portela, *J. Catal.*, 1996, 164, 399-410.
31. F. Y. A. El Kady, S. A. Shaban and A. O. Abo El Naga, *Transition Met. Chem.*, 2011, 36, 237-244.
32. X. Q. Wang and U. S. Ozkan, *J. Mol. Catal. A: Chem.*, 2005, 232, 101-112.
33. P. Dufresne, E. Payen, J. Grimblot and J. P. Bonnelle, *J. Phys. Chem.*, 1981, 85, 2344-2351.
34. G. Mestl, *J. Mol. Catal. A: Chem.*, 2000, 158, 45-65.
35. H. C. Hu and I. E. Wachs, *J. Phys. Chem.*, 1995, 99, 10911-10922.
36. D. S. Kim, K. Segawa, T. Soeya and I. E. Wachs, *J. Catal.*, 1992, 136, 539-553.
37. G. Mestl and T. K. K. Srinivasan, *Catal. Rev. Sci., Eng.*, 1998, 40, 451-570.
38. S. L. González-Cortés, T. C. Xiao, P. M. F. J. Costa, B. Fontal and M. L. H. Green, *Appl. Catal., A*, 2004, 270, 209-222.
39. C. Lamonier, C. Martin, J. Mazurelle, V. Harlé, D. Guillaume and E. Payen, *Appl. Catal., B*, 2007, 70, 548-556.
40. A. N. Desikan, L. Huang and S. T. Oyama, *J. Phys. Chem.*, 1991, 95, 10050-10056.
41. L. Fang, S. P. Xu, L. Cao, Y. Chi, T. Zhang and D. F. Xue, *J. Phys. Chem. C*, 2007, 111, 7396-7402.
42. J. C. M. Th. Weber , J. H. M. C. van Wolput , C. P. J. Verhagen , and J. W. Niemantsverdriet *J. Phys. Chem.*, 1996, 100, 14144-14150.
43. T. K. T. Ninh, L. Massin, D. Laurenti and M. Vrinat, *Appl. Catal., A*, 2011, 407, 29-39.
44. R. Hernández-Huesca, J. Mérida-Robles, P. Maireles-Torres, E. Rodríguez-Castellón and A. Jiménez-López, *J. Catal.*, 2001, 203, 122-132.
45. S. W. A. Galtayries, J. Grimblot, *J. Electron. Spectrosc. Relat. Phenome.*, 1997, 87, 31-44.
46. B. Guichard, M. Roy-Auberger, E. Devers, C. Legens and P. Raybaud, *Catal. Today*, 2008, 130, 97-108.
47. J. Escobar, M. C. Barrera, J. A. Toledo, M. A. Cortés-Jácome, C. Angeles-Chávez, S. Núñez, V. Santes, E. Gómez, L. Díaz, E. Romero and J. G. Pacheco, *Appl. Catal., B*, 2009, 88, 564-575.
48. H. R. Reinhoudt, A. D. van Langeveld, P. J. Kooyman, R. M. Stockmann, R. Prins, H. W. Zandbergen and J. A. Moulijn, *J. Catal.*, 1998, 179, 443-450.
49. J. L. Brito and J. Laine, *Appl Catal*, 1991, 72, L13-L15.
50. S. Chaturvedi, J. A. Rodriguez and J. L. Brito, *Catal. Lett.*, 1998, 51, 85-93.
51. J. G. Kushmerick and P. S. Weiss, *J. Phys. Chem. B*, 1998, 102, 10094-10097.